Sensitivity Analysis of Commutation Failure in Multi-Infeed HVDC Systems: Exploring the Impact of ac System Representations and Fault Types

Jhair S. Acosta, Hao Xiao and Aniruddha M. Gole
Department of Electrical and Computer Engineering, University of Manitoba, Winnipeg, Canada
{jhair.acostasarmiento1*, Hao.Xiao1*, Aniruddha.Gole}@umanitoba.ca

***Abstract*—This paper investigates commutation failure (CF) in line commutated HVdc converters within multi-infeed HVDC systems and thereby provides valuable insights for the operation and design of HVdc systems. CF susceptibility across various operational scenarios, fault types, and ac system representations at different frequencies is explored. An Electromagnetic Transients (EMT) model is constructed and parameter changes are applied using Monte-Carlo Simulation. The process is fully automated with the use of a controlling program written in Python, which varies parameter values and facilitates result retrieval and post-simulation analysis. A typical analysis results in several hundred thousands of simulation runs, requiring the procedure to be implemented on a parallel computing platform. The results show that two-phase faults are the most critical CF triggers, an aspect often overlooked in previous literature focused on three-phase or single-phase-to-ground faults. Furthermore, the frequency dependent characteristics of the ac network can result in very different CF susceptibilities.**

***Index Terms*—Electromagnetic Transient Simulation, High Performance Computing, Multi-infeed systems.**

I. Introduction

Modern power systems are seeing an increasing use of High Voltage Direct Current Transmission to connect remote ac networks, due to its beneficial properties such as the ability to connect grids asynchronously, lower transmission losses, etc. Although Voltage Sourced Converters (VSCs) are seeing increasing use, there is still a very large number of line-commutated converter-based HVdc (LCC-HVdc) systems, particularly for use in long-distance bulk power transmission. As a result, it is becoming common to have "Multi-infeed" systems in which multiple LCC inverters terminate in close proximity [1], [2]. In such systems, the voltage support provided by the ac network is shared between multiple converters and so each individual inverter appears to be connected to a weaker ac network in comparison to situations where the other inverters are absent [3], [4]. LCC-HVdc systems can experience commutation failures (CF) , i.e., the failure of the current to transfer from a conducting valve to the next in conduction sequence. The primary cause of CF is insufficient ac system strength, usually expressed as a Short Circuit Ratio (SCR). This strength degradation can result in an increase in CF risk [5], [6] and consequently in potential grid instability. The CFs can be local (where the CF occurs only on one converter) or concurrent, where it spreads to multiple converters in the grid. Thus, an efficient and comprehensive analysis of the CF behaviour is beneficial for subsequently undertaking remedial countermeasures.

Earlier CF studies in multi-infeed systems have been primarily devoted to two types of methods. The first is an analytical method based on the inverter's quasi-steady-state equations to predict the local and concurrent CF onset when the calculated inverter ac bus voltage depression is below the critical one [7], [8]. The other is to employ electromagnetic transient (EMT) simulations for the observation of the CF phenomenon such as the obviously reduced extinction angle or increased dc current [2], [9]. Analytical studies usually considered symmetrical ac faults, although recently Song et al have also considered double-phase faults [10]. However, as CF is a highly non-linear phenomenon, analytical methods cannot adequately handle the range of different potential system conditions. On the other hand, EMT simulation is more accurate as the detailed commutation process in the thyristor valve and hence the non-linearity of the CF are modelled in great detail [11].

To quantify the severity of CF, a probabilistic measure known as the commutation failure immunity index (CFII) is widely used [2]. CFII is determined through EMT simulations by applying faults at different points on the waveform. The CFII then is the ratio of the number of instances in which CF did not occur. A large CFII indicates more immunity to CFs. Also, a critical fault level can be defined as the maximum local fault level that inverters can withstand without having a CF.

Previous publications have reported that the local CF is largely affected by the effective short-circuit ratio (ESCR) seen from the local inverter ac bus into the common grid. CIGRE WG B4.41 [1] has defined the Multi-infeed interaction Factor between converters connected to ac buses i and j as $MIIF_{i,j} = |\Delta V_j|/|\Delta V_i|$, where ΔV_i is a small voltage reduction applied at bus i, and ΔV_j is the corresponding voltage reduction at bus j. MIIF quantifies the inter-inverter interaction strength [2]. Concurrent CF has shown to be affected by both the MIIF and the local ESCR, whereas local CFII is not significantly affected by the MIIF. Additionally,

Submitted to the 23^{rd} Power Systems Computation Conference (PSCC 2024).
* Corresponding authors

concurrent CFII may exhibit anomalous behaviour in which a less severe fault may cause CF, whereas a slightly more serious one may not. This has been attributed to voltage distortion [2], [12]; for various reasons, including the propagation of harmonics from the local bus to the remote inverters triggered by a CF [12], [13].

Existing investigations have demonstrated that CF depends on various factors, such as the strength of the ac systems, the voltage depression and harmonics generated after a fault in the ac side, and the fault element [2], [14]–[18]. However, these studies primarily applied symmetrical faults, which are not the most frequent fault type [19]. Additionally, as this paper will show, they are also not the most severe fault type, as far as CF phenomena are concerned.

This paper addresses the following gaps not covered in earlier work: 1) Previous research has predominantly focused on the use of fundamental frequency ac grid impedance representations, neglecting the potential influences arising from frequency-dependent characteristics. 2) It considers three-phase faults as the most serious ones, whereas this paper will show that two phase faults are the real onerous ones. 3) While the analytical impact of two-phase faults on valve commutation in single-infeed systems has been examined in [10], those results cannot be easily extrapolated to multi-infeed system scenarios due to the intricate interactions between inverters [15], [20], [21].

The paper makes the following main contributions:

- Development of an automated tool for comprehensive analysis of CF behavior through parallel EMT simulations utilizing all available cores.
- In-depth investigation of CF behavior encompassing diverse ac network representations and fault types.

The investigation highlight the following behaviours: i) Two-phase faults are the most critical CF triggers in multi-infeed systems and ii) The manner in which the frequency response of the ac network is modeled greatly affects the CF behaviour.

II. Commutation Failure

Commutation failure (CF) in LCC inverters is the inability of the current to transfer (commutate) from one thyristor valve to the next in the firing sequence [8]. This is a consequence of a reduction in the valve extinction angle that may be caused by a voltage magnitude depression, phase shift, voltage distortion at the inverter ac bus, or dc current. It is a nuisance phenomenon that can lead to power transfer interruption and sometimes a shutdown of the system [22]–[24].

CF can be detected by comparing the instantaneous sum of valve winding side ac currents i_a, i_b, i_c with the dc current I_{dc}. In a normally operating LCC, the currents must satisfy (1). CF is flagged by the sum of the currents on the left hand side of (1) exceeding the right hand side.

$$|i_a| + |i_b| + |i_c| = |2I_{dc}| \tag{1}$$

Typically, CF is more prone to happen for more severe faults. The severity of a fault at node i is a function the fault impedance z_f. In existing literature, it is quantified by a "fault level", as defined by (2) where V_i is the voltage at node i. However, a more meaningful value is obtained by expressing the fault level as a normalized quantity by dividing it by the converter power (Pdc_i) as in (3).

$$F_{lvl} = \frac{V_i^2}{z_f} \tag{2}$$

$$Fr_{lvl} = 100\frac{F_{lt_lvl}}{Pdc_i} \tag{3}$$

CF is also affected by the point on wave at which the fault occurs. However, by conducting exhaustive simulations, it is possible to find a critical value of fault severity $Fr_{lvl} = F_{critical}$ such that any less severe fault does not result in a CF regardless of the point on wave of fault application. This fault level can be used to define a "commutation failure immunity index" (CFII) (4) [2], [14]. A larger CFII indicates that the inverter can tolerate more sever faults, i.e., it is less susceptible to commutation failures.

$$CFII = F_{critical} \tag{4}$$

Note that calculating the CFII requires a large number of simulations, which is an inefficient and very time-consuming process. Therefore, the development of an efficient automated simulation tool that can conduct several simulations and come up with a CFII value without human intervention is desirable. This is particularly true if multiple operating scenarios and loading levels are to be investigated.

III. Automated Simulation Tool

A Python code wrapper was developed for an EMT program (PSCAD, in this case) to automatically run the large number of EMT simulations required to perform CF studies in multi-infeed systems. It was implemented to utilize parallel computing in an efficient way, so that multiple simulations could be run in parallel. The created program uses a simple interface (Fig. 1) to select different parameters such as the desired system, fault types, elements, range, etc.; to perform the study using parallel computing and then analyze and plot the results. In a summarized form, the program follows the the process shown in the flowchart in Fig. 2.

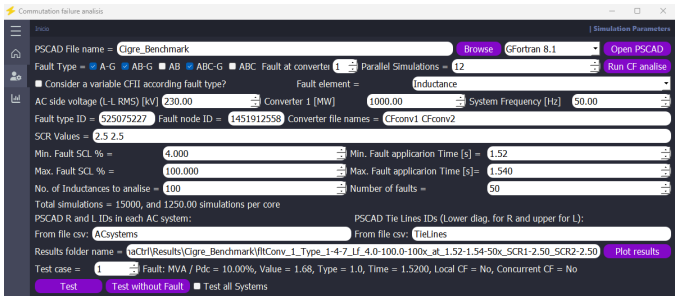

Fig. 1. Automation program interface.

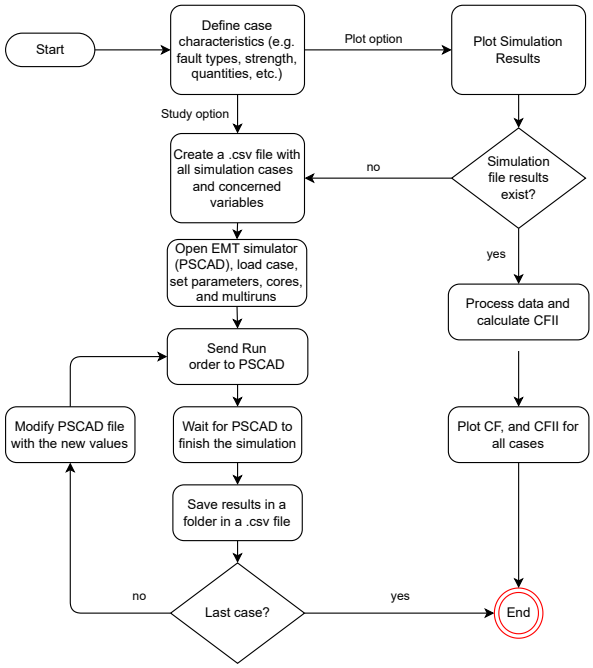

Fig. 2. Automation program flowchart.

To conduct the parallel simulations, a custom component labeled *Parallel Controller* was developed and embedded into PSCAD as shown in Fig. 3. The component is able to distribute the computation load among all available cores on the computing platform by applying (5). This component outputs a case number for assigning an individual simulation to a specific computing core (identified by $coreNo$) according to (5). It also considers the total number of simulations per core ($tRuns$), and the current simulation at the core ($currentRun$). A lookup table ($Lfvalues.out$), generated using the Python interface on Fig. 1 is then consulted by PSCAD to select the simulation parameters such as fault type, fault inductance, fault instant, etc., to be used for that run. This ensures that all the processors are used during the parallel simulation and that the correct parameters are selected.

$$case = (coreNo - 1) * tRuns + currentRun \qquad (5)$$

Graphically, the custom controller component is as in Fig. 3. As it can be inferred, each case will correspond to a different value of fault type, fault element value, and fault incidence time. With this component, it is possible to simulate in parallel as many cases as the PSCAD license and hardware limitations in the machine allows.

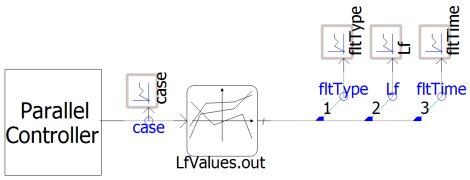

Fig. 3. Custom parallel simulations controller in PSCAD.

For comparison purposes, Table I presents the simulation time under different conditions. As you can note, the individual speed of each processor is an important factor. Thus, even when simulating batches of 64 cases in parallel in a slower machine, the simulation time is higher than when simulating batches of 12 parallel cases in a faster machine. However, note that the total number of simulations is slightly different in all cases. This is because to be able to make the simulations in parallel, the total number of cases to be simulated must be a multiple of the number of simulations to run in parallel.

TABLE I
COMPARISON OF PARALLEL SIMULATIONS IN TWO DIFFERENT COMPUTERS.

PC type	32 core	6 core	6 core
Speed (GHz)	2.1	3.4	3.4
No. of Parallel simulations	64	8	12
Cases simulated per fault type	2816	2800	2808
Total cases simulated	8448	8400	8424
Wall-clock time (minutes)	124	168	115

IV. TEST SYSTEM AND CF STUDY

The dual-infeed LCC-HVdc configuration in Fig. 4, is used to analyze the CF behaviour. The data for each HVdc link, including the ac filters is as in the CIGRE HVdc Benchmark Model [25], [26]. The ac buses for each of the 12-pulse LCC converters in the common receiving end ac grid are interconnected by a Tie line. Each 12-pulse converter is composed of two 6-pulse converters with valve parameters as shown in Table III. Each rectifier operates in the constant dc current control mode and each inverter in the constant extinction angle control mode with a reference extinction angle of 15^o. The controller structure is shown in Fig. 5 and its parameters are given in Table II. Also, other test system parameters are presented in Table IV.

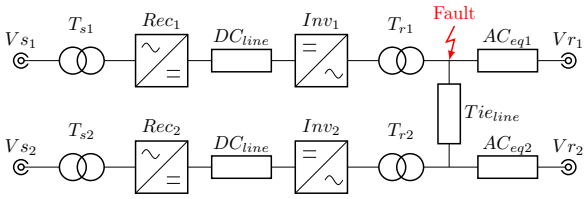

Fig. 4. Multi-infeed system representation.

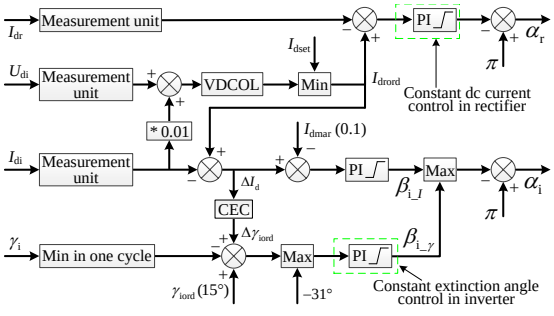

Fig. 5. HVdc controller diagram.

TABLE II
PI CONTROLLER PARAMETERS OF HVDC CONVERTERS.

PI controller	Proportional gain	Integral time constant [s]
dc current control in rectifier	1.0989	0.01092
Extinction angle control in inverter	0.7506	0.0544

TABLE III
VALVE PARAMETERS.

Valve Parameter	Value
Thyristor ON resistance	0.01 [Ω]
Thyristor OFF resistance	100000000.0 [Ω]
Forward voltage drop	0.0 [kV]
Forward breakover voltage	100000.0 [kV]
Reverse withstand voltage	100000.0 [kV]
Minimum extinction time	0.0 [us]
Snubber resistance	5000.0 [Ω]
Snubber capacitance	0.05 [μF]

TABLE IV
MULTI-INFEED TEST SYSTEM CHARACTERISTICS CONSIDERING AN OPERATION FREQUENCY OF 50 HZ.

Converters		
	Rectifier	Inverter
Power [MW]	1000	1000
dc Voltage [kV]	500	500
Firing/extinction angle [°]	$\alpha = 15$	$\gamma = 15$
Shunt Filters		
Apparent power [MVA]	125	
Harmonic Filters		
Harmonic	11^{th}	13^{th}
Apparent power [MVA]	252	252
Transformers		
Winding voltages [kV]	345/426.92	418.46/230
Apparent power [MVA]	1207.46	1183.58
Positive Leakage reactance [pu]	0.18	0.18
DC Line		
	First half	Second Half
Inductance [H]	0.5968	0.596
Resistance [Ω]	2.5	2.5
Capacitance [μF]	26	
AC Systems		
	Rectifier side	Inverter side
SCR	$2.5\angle 84°$	$2.5\angle 75°$
Source Voltage [kV]	382.87	215.05
Tie Line (Modeled as an RL)		
Resistance [Ω]	5.39	
Inductance [mH]	102.99	

A. *Impact of the fault type*

As has been reported in the CIGRE Guide on Multi-infeed systems [1] and other previous literature [27], inductive faults have been identified to be more severe than resistive faults. This was also confirmed in the proposed model, although for the sake of compactness, only the most severe (inductive) faults are presented here.

Permanent inductive single (A-G), double (AB and AB-G), and three-phase (ABC-G) faults were applied at the converter ac busbar as shown in Fig. 4. The fault application time was uniformly varied over one ac cycle (50 Hz) by dividing the fundamental period into 50 equal steps. Also, the fault severity was varied by using 100 different fault levels ranging from 100 MVA (0.1 in normalized units) to 2500 MVA (2.5 in normalized units).

The probability plots for local CFs showing CFII as a function of fault severity level, are presented in Fig. 6. As can be seen, the local CFIIs are 24.5, 17.4, 18.7, and 15.4 %, which corresponds to fault levels of 245, 174, 187, and 154 MVA respectively. Therefore, it is evidenced that the two-phase fault is the most onerous as it has the lowest local CFII.

Similarly, the plots of CFII values for concurrent CF are shown in Fig. 7. Once again, the concurrent CFII for the two-phase fault is the lowest compared to the other fault types. This highlights the importance of considering two-phase faults in CF studies. However, earlier research has always considered the three-phase fault as the most troublesome for the CF assessment in the multi-infeed systems [1], [2].

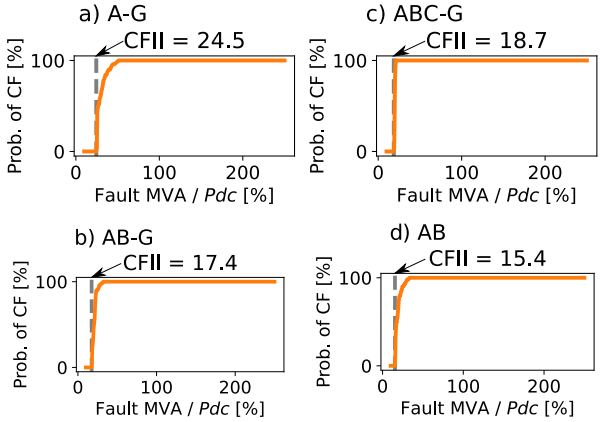

Fig. 6. Local CF probability when applying A-G, AB-G, ABC-G, and AB faults.

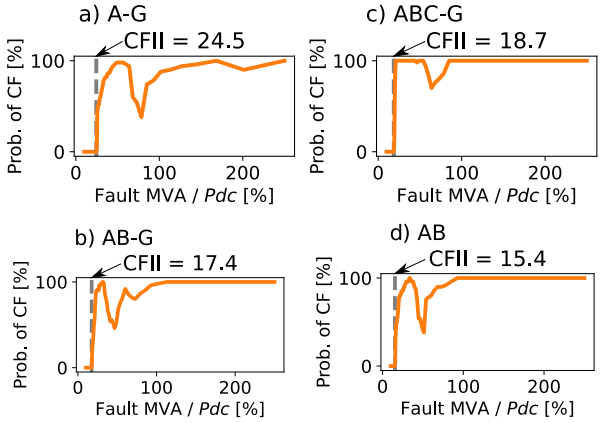

Fig. 7. Concurrent CF probability when applying A-G, AB-G, ABC-G, and AB faults.

1) Rationalization of the observations: Simulations showed (not plotted) that the ac line-line voltage in the commutating phases is in fact marginally larger than for the three-phase fault at both inverter ac buses 1 and 2, so if voltage depression were the root cause of CF, one should expect little or no difference in CFII values. However, the results show a smaller CFII for the 2-phase fault. Looking at the voltage waveform closely shows that the two-phase fault induces a larger zero-crossing

phase shift of the line-to-line voltage and thereby reduces the area under the commutating voltage curve, resulting in a higher probability of CF [8], [10]. Hence, the resulting extinction angle γ for the converter is actually smaller than the value γ_{ss} obtained from the quasi-steady-state calculation expression by a small angle ($\Delta\phi$) as shown in (6). Here, X_T is the inverter transformer leakage reactance, and β is the inverter advance firing angle. The greater the reduction in γ the higher the risks of both local and concurrent CF, i.e., the lower the CFII.

$$\begin{aligned} \gamma_1 &= arccos\left(\frac{X_T I_d}{1-\Delta U+cos\beta}\right) \\ \gamma &= \gamma_1 - \Delta\phi \end{aligned} \tag{6}$$

B. Impact of the ac system equivalent representation

The majority of previous CF studies in HVdc systems have represented the ac network as a Thevenin equivalent, with the Thevenin impedance Z_{th} selected as the fundamental frequency ac grid impedance which is quantified by the SCR or ESCR expressions in (7) and (8). Here, Qf_i is the reactive power compensation at the inverter ac bus.

$$SCR_i = \frac{V_i^2}{Z_{th}Pdc_i} \tag{7}$$

$$ESCR_i = \frac{\frac{V_i^2}{Z_{th}} - Qf_i}{Pdc_i} \tag{8}$$

However, the impact of the frequency-dependent characteristics of various ac grid representations on the CF behaviors in the multi-infeed system is not clear. Thereby, this section further investigates how the local and concurrent CF probability is affected by several different ac grid representations shown in Figs. 8-12. All the equivalents have the same impedance at fundamental frequency giving an SCR value of $2.5\angle 75°$.

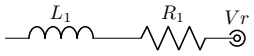

Fig. 8. AC system represented as a R-L equivalent, with $R_1 = 5.48\Omega$ and $L_1 = 65.06$mH.

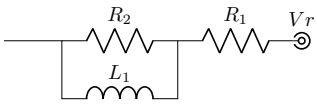

Fig. 9. AC system represented as an arrange of $R-R||L$ in elements, with $R_1 = 4.79\Omega$, $R_2 = 615.29\Omega$, and $L_1 = 65.10$mH.

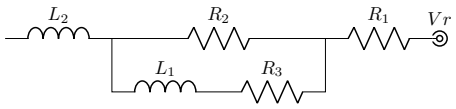

Fig. 10. AC system represented as in the CIGRE benchmark [25], with $R_1 = R_3 = 0.7406\Omega$, $R_2 = 24.81\Omega$, and $L_1 = L_2 = 36.5$mH.

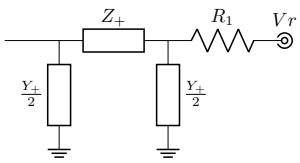

Fig. 11. AC system represented as a resistance ($R_1 = 3.8\Omega$) in series with a 48.8 km π transmission line, with $R_+ = 34.33\mu\Omega/m$, $Xl_+ = 0.42m\Omega/m$, $Xc_+ = 364.419M\Omega * m$, $R_0 = 291.27\mu\Omega/m$, $Xl_0 = 1.15m\Omega/m$, and $Xc_0 = 531.208M\Omega * m$.

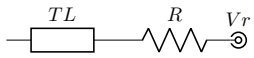

Fig. 12. AC system represented as a 48.8 km transmission line plus a resistance of 3.8Ω.

The first representation (Fig. 8) corresponds to a simple $R-L$ arrangement. The second (Fig. 9) to a $R-R||L$ circuit with impedance angle of $75°$ at fundamental and 7^{th} harmonic. Such a network is often used when the ac network is modelling transient behaviour. The third representation (Fig. 10) is the same RL circuit used in the CIGRE benchmark model [25], which also has an impedance angle of $75°$ at fundamental and 7^{th} harmonics. Finally, the fourth and fifth options simulate the case of a 49 km length 230 kV transmission line incident at the converter bus, modelled either as a π model (Fig. 11) or as a frequency dependent parameter line (Fig. 12), with the data presented in Table V.

TABLE V
SEQUENCE COMPONENTS OF THE TRANSMISSION LINE IN PU USING 230.00 KV (L-L) AND 100.00 MVA AS BASE.

	Zero Sequence	Positive Sequence
Resistance	0.268701394E-01	0.316717767E-02
Reactance	0.106698604	0.386352270E-01
Susceptance	0.485971334E-01	0.708392806E-01
Surge Impedance	1.48174695	0.738507080

Fig. 13 shows the positive sequence impedance variations of these ac grid representations as a function of frequency. It is evident that all representations coincide at the fundamental frequency, but demonstrate considerably different frequency-dependent behaviours.

Fig. 14 shows the behaviour of the local (a, c, e, g, and i) and concurrent (b, d, f, h, and j) CF probability and CFII values obtained with the different ac system representations of Figs. 8-12, for the line-line faults, which were shown in Section IV-A to be the most serious ones. Note that the shape of the CF probability response in Fig. 14 is similar in all ac system representations. Both local and concurrent CFII values vary depending on the representation used, but the largest values of 15.4 occurs for for the CIGRE ac system representation of Fig. 10. All the other equivalents show lower, nearly equal CFIIs between 13.4 and 13.9.

Additionally, Fig. 15 shows the CFII for the ac representations under single, double, and three-phase faults. Once again, it is evidenced that the CIGRE ac representation

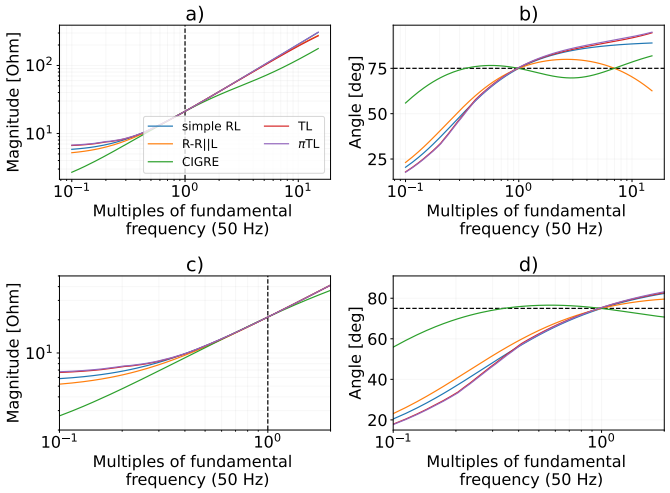

Fig. 13. Positive sequence magnitude (a) and angle (b) of the ac system equivalents for different frequencies. Zoom of the magnitude (c) and angle (d).

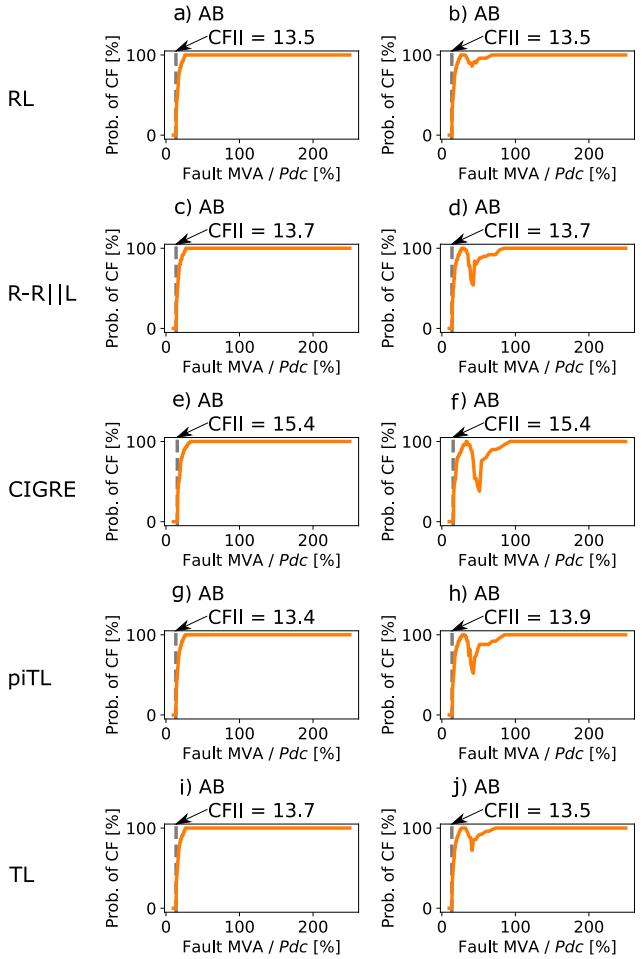

Fig. 14. Local and concurrent CF probability and CFII for the ac system representations, when applied an AB-G fault.

has the highest CFII and that the most severe faults (lowest CFII) are the two-phase faults.

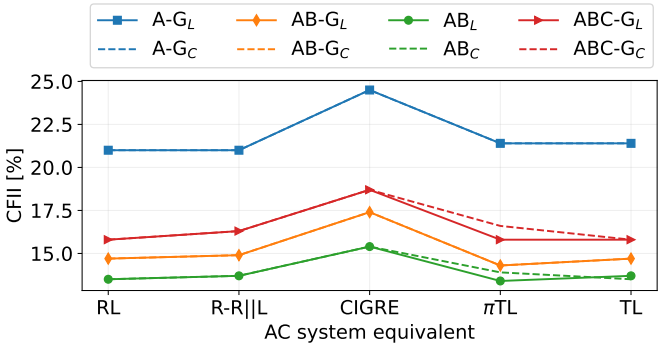

Fig. 15. Local ($_L$) and concurrent ($_C$) CFII for each ac system representation and different fault types.

1) Rationalization of the observations: The observations can be rationalized as given below. As shown in Fig. 13, the magnitude of the harmonic impedance (Z_h) in the CIGRE equivalent is significantly smaller than the other four ac grid representations in the low-frequency range (see Fig. 13 (a) and (c)) which have roughly similar low frequency impedances. The ac fault results in an asymmetry in the injected currents I_h into the ac network, which are typically rife with low-order harmonics, being typical the 2^{nd} and 3^{rd} [16]. This results in low order voltage harmonic components $V_h = Z_h I_h$. If Z_h is small, as is the case in the CIGRE equivalent, the distortion is smaller as well. This results in the higher CFII values.

C. Assessment Under Different ac Grid Strength

In the previous section, all ac system representations had the same fundamental frequency SCR of $2.5\angle 75°$. In this section, the CF behaviour is investigated as a function of varying ac grid strengths. In order to do this, SCR_1 and SCR_2 for inverters 1 and 2 are varied between 2.0 to 5.0. For each combination of SCRs, the CFII values are obtained using the developed automation tool. The local CFII results for single-phase A-G, two-phase (AB) and three-phase to ground (ABC-G) are presented in Figs. 16 to 18. The corresponding results for the concurrent CFII are shown in Figs. 19 to 21.

A first observation of Figs. 16-21, evidence that the AB fault remains to be the worst, leading to low local and concurrent CFII, no matter the SCRs combination. Another observation on the local CF is that the local CFII is primarily affected by SCR_1 but hardly influenced by SCR_2, no matter the ac fault type. More precisely, a larger SCR_1 always means a higher local CFII value. However, the concurrent CF behavior is dependent on both SCRs. This is expected since a higher SCR_2 indicates a reduced interaction from inverter 1 to 2 as quantified by the $MIIF_{21}$ [2]. The simplified computation expression of the $MIIF_{21}$ is given in (9) [13], where Z_{21} is the nodal mutual-impedance matrix element between inverter ac buses 2 and 1, and Z_{11} is the nodal self-impedance matrix element for inverter ac bus 1. Therefore, a reduced $MIIF_{21}$ implies a lower risk of concurrent CF.

$$MIIF_{21} = \frac{Z_{21}}{Z_{11}} \tag{9}$$

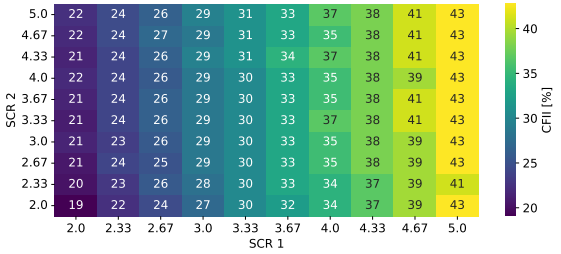

Fig. 16. Variation of the Local CFII according to the SCR for A-G faults.

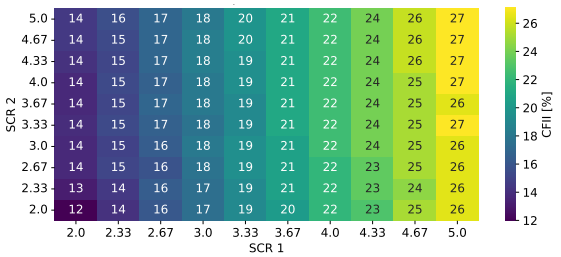

Fig. 17. Variation of the Local CFII according to the SCR for AB faults.

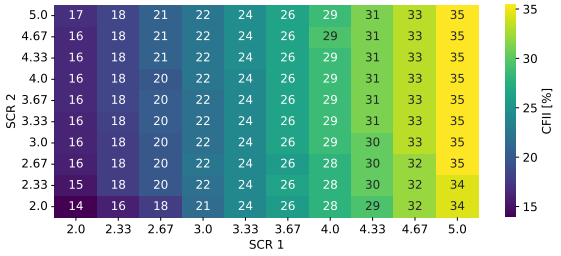

Fig. 18. Variation of the Local CFII according to the SCR for ABC-G faults.

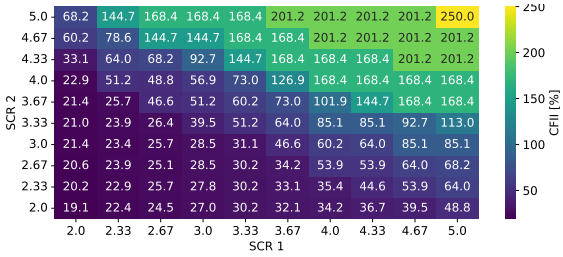

Fig. 19. Variation of the Concurrent CFII according to the SCR for A-G faults.

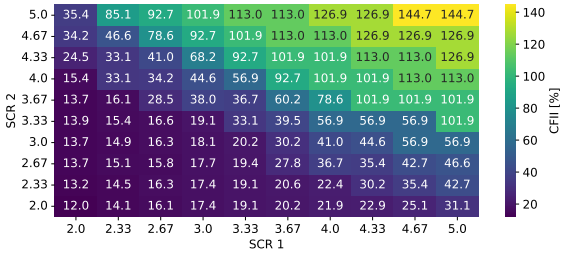

Fig. 20. Variation of the Concurrent CFII according to the SCR for AB faults.

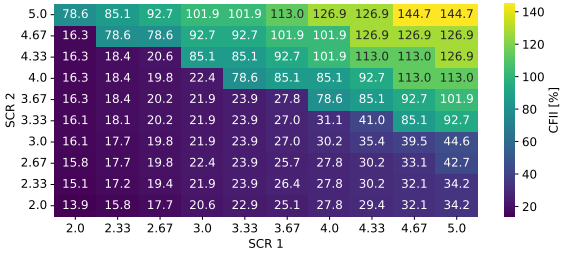

Fig. 21. Variation of the Concurrent CFII according to the SCR for ABC-G faults.

V. Conclusions

The paper assesses local and concurrent commutation failure (CF) behaviour in multi-infeed HVdc systems. Most previous research quantified the connecting ac network using the short circuit ratio, which is inversely proportional to the fundamental frequency impedance of the ac source's Thevenin equivalent. However, this study reveals that different network representations, such as simple R-L equivalents, complex Thevenin equivalents, and others with converter bus connections to remote networks through transmission lines, can significantly affect CF behavior, even when all representations have the same fundamental frequency impedance.

The ac representation in the CIGRE benchmark model is shown to give overly optimistic results compared with other impedance representations, which manifest a higher susceptibility to CFs. Furthermore, the paper extends the analysis to asymmetrical faults and concludes that line-to-line faults are the most severe in terms of CF, surpassing three-phase-to-ground faults. This conclusion holds across various ac system representations, short circuit ratios, and local or concurrent CF scenarios. Consequently, the paper emphasizes the importance of including line-to-line faults in CF assessment, challenging the previous reliance on three-phase faults alone in existing literature.

References

[1] CIGRE WG B4.41, "Systems with multiple DC infeed," CIGRE working group 364, Tech. Rep. December, 2008.

[2] E. Rahimi, A. M. Gole, J. B. Davies, I. T. Fernando, and K. L. Kent, "Commutation Failure Analysis in Multi-Infeed HVDC Systems," *IEEE Transactions on Power Delivery*, vol. 26, no. 1, pp. 378–384, jan 2011. [Online]. Available: http://ieeexplore.ieee.org/document/5673966/

[3] D. H. A. Lee and G. Andersson, "An equivalent single-infeed model of multi-infeed hvdc systems for voltage and power stability analysis," *IEEE Transactions on Power Delivery*, vol. 31, no. 1, pp. 303–312, 2016.

[4] B. Y. Lee, J. K. Park, S. H. Myung, S. W. Min, and E. S. Kim, "An effective modelling method to analyze electric field around transmission lines and substations using a generalized finite line charge," *IEEE Trans. Power Deliv.*, vol. 12, no. 3, pp. 1143–1149, 1997.

[5] H. Huang, Z. Xu, and X. Lin, "Improving performance of multi-infeed hvdc systems using grid dynamic segmentation technique based on fault current limiters," *IEEE Transactions on Power Systems*, vol. 27, no. 3, pp. 1664–1672, 2012.

[6] R. Hong, X. Shukai, Z. Yong, H. Chao, and W. Wei, "Research and application of multiple statcoms to improve the stability of ac/dc power systems in china southern grid," *IET Generation, Transmission & Distribution*, vol. 10, pp. 3111–3118(7), October 2016.

[7] Y. Zhou, H. Wu, W. Wei, Y. Song, and H. Deng, "Optimal allocation of dynamic var sources for reducing the probability of commutation failure occurrence in the receiving-end systems," *IEEE Transactions on Power Delivery*, vol. 34, no. 1, pp. 324–333, 2019.

[8] C. Thio, J. Davies, and K. Kent, "Commutation failures in hvdc transmission systems," *IEEE Transactions on Power Delivery*, vol. 11, no. 2, pp. 946–957, 1996.

[9] S. Mirsaeidi, X. Dong, and D. M. Said, "A fault current limiting approach for commutation failure prevention in lcc-hvdc transmission systems," *IEEE Transactions on Power Delivery*, vol. 34, no. 5, pp. 2018–2027, 2019.

[10] J. Song, Y. Li, Y. Zhang, and J. Zhang, "Influence of transition resistance and fault moment on DC system commutation process caused by twophase fault of AC system," *The Journal of Engineering*, vol. 2019, no. 16, pp. 1306–1312, 2019.

[11] X. Chen, A. M. Gole, and M. Han, "Analysis of mixed inverter/rectifier multi-infeed hvdc systems," *IEEE Transactions on Power Delivery*, vol. 27, no. 3, pp. 1565–1573, 2012.

[12] H. Xiao, Y. Li, A. M. Gole, and X. Duan, "Computationally efficient and accurate approach for commutation failure risk areas identification in multi-infeed lcc-hvdc systems," *IEEE Transactions on Power Electronics*, vol. 35, no. 5, pp. 5238–5253, 2020.

[13] Y. Shao and Y. Tang, "Fast evaluation of commutation failure risk in multi-infeed hvdc systems," *IEEE Transactions on Power Systems*, vol. 33, no. 1, pp. 646–653, 2018.

[14] E. Rahimi, A. M. Gole, J. B. Davies, I. T. Fernando, and K. L. Kent, "Commutation failure in single- and multi-infeed HVDC systems," in *8th IEE International Conference on AC and DC Power Transmission (ACDC 2006)*, vol. 2006, no. I. IEE, 2006, pp. 182–186.

[15] D. L. H. Aik and G. Andersson, "Analysis of voltage and power interactions in multi-infeed HVDC systems," *IEEE Transactions on Power Delivery*, vol. 28, no. 2, pp. 816–824, 2013.

[16] F. Wang, T. qi Liu, and X. yuan Li, "Decreasing the frequency of HVDC commutation failures caused by harmonics," *IET Power Electronics*, vol. 10, no. 2, pp. 215–221, 2017.

[17] Q. Wang, C. Zhang, X. Wu, and Y. Tang, "Commutation failure prediction method considering commutation voltage distortion and dc current variation," *IEEE Access*, vol. 7, pp. 96 531–96 539, 2019.

[18] B. Rehman, A. U. Rehman, W. A. Khan, I. Sami, and J.-S. Ro, "Operation and Challenges of Multi-Infeed LCCHVDC System: Commutation Failure, AC/DC Power Flow, and Voltage Stability," *Applied Sciences*, vol. 11, no. 18, p. 8637, sep 2021. [Online]. Available: https://www.mdpi.com/2076-3417/11/18/8637

[19] O. Dias and M. C. Tavares, "Comparison between traditional single-phase auto reclosing and adaptive technique based on harmonic content measurement," *IET Generation, Transmission and Distribution*, vol. 11, no. 4, pp. 905–914, 2017.

[20] C. Guo, Y. Zhang, A. M. Gole, and C. Zhao, "Analysis of dual-infeed hvdc with lcchvdc and vschvdc," *IEEE Transactions on Power Delivery*, vol. 27, no. 3, pp. 1529–1537, 2012.

[21] Y. Xue, X.-P. Zhang, and C. Yang, "Commutation failure elimination of lcc hvdc systems using thyristor-based controllable capacitors," *IEEE Transactions on Power Delivery*, vol. 33, no. 3, pp. 1448–1458, 2018.

[22] G. Kristmundsson and D. Carroll, "The effect of ac system frequency spectrum on commutation failure in hvdc inverters," *IEEE Transactions on Power Delivery*, vol. 5, no. 2, pp. 1121–1128, 1990.

[23] W. Yao, C. Liu, J. Fang, X. Ai, J. Wen, and S. Cheng, "Probabilistic analysis of commutation failure in lcc-hvdc system considering the cfprev and the initial fault voltage angle," *IEEE Transactions on Power Delivery*, vol. 35, no. 2, pp. 715–724, 2020.

[24] Z. Wei, Y. Yuan, X. Lei, H. Wang, G. Sun, and Y. Sun, "Direct-current predictive control strategy for inhibiting commutation failure in hvdc converter," *IEEE Transactions on Power Systems*, vol. 29, no. 5, pp. 2409–2417, 2014.

[25] M. Szechtman, T. Wess, and C. Thio, "A benchmark model for hvdc system studies," in *International Conference on AC and DC Power Transmission*, 1991, pp. 374–378.

[26] M. Szechtman, "First benchmark model for hvdc control studies," in *Electra*, vol. 135, 1991, pp. 54–73.

[27] E. Rahimi, A. Gole, J. Davies, I. Fernando, and K. Kent, "Commutation failure in single- and multi-infeed hvdc systems," in *The 8th IEE International Conference on AC and DC Power Transmission*, 2006, pp. 182–186.